2019 SECED Conference
Earthquake risk and engineering towards a resilient world
9-10 September 2019, Greenwich, London

Parametric Study for Shear and Flexural Simplified Formulations for Spandrels in Unreinforced Masonry (URM) Elements

Hasan AYOUBY[1], Ashutosh BAGCHI[2] & LuciaTIRCA[3]

Abstract: *The seismic modeling of URM buildings is characterized by its complexity due to the large number of variables that define the structural elements. This would restraint the analysis to specific construction types leading to conservative assessment of the structure. To understand the behavior of URM structures during earthquakes, models that can simulate their response accurately are developed. Utilizing the equivalent frame technique as a simplified method for reducing the complexity of such buildings requires the use of capacity formulations that are assigned as hinges at specific locations of the defined elements. Following up on a previous parametric study that tackles the dominant shear and flexural failures in piers, this work focuses on the in-plane behavior of spandrels and their corresponding simplified formulations present in the literature. The formulations are calibrated against experimental campaigns to verify their efficiency in representing the various parameters in masonry panels. Variations in the geometrical aspects of spandrels, type of construction, materials and loadings are important factors in determining the outcomes of the lateral response. It is noticed that each equation has a different degree of accuracy with respect to the different parameters which indicates the need to implement all of them in the analyses to maintain a comprehensive simulation of the global behavior of the masonry wall. A future practice will include automating the latter parametric studies in an open source software predicated on increasing the volume of such information as more research is achieved thus increasing the accuracy of the results over time.*

Introduction

Spandrels are considered as secondary elements in URM walls, however they significantly contribute to the overall seismic response. Through the connective joints, spandrels form a coupling effect on the adjacent piers determining their boundary conditions and the stress distribution along their spans (Foraboschi, 2009). In many codes, simplified equivalent frame models are allowed to used utilize the “weak spandrel strong piers” approach which ignores the spandrels thus considering the piers as cantilevers and “strong spandrels weak piers” approach which models the spandrel as a rigid element thus considering the piers as fixed-fixed elements (Cattari & Lagomarsino, 2008). The two approaches do not fully represent the actual behavior of spandrels that can experience a variation of strength and ductility throughout the ground motion application. Therefore modeling the strength capacities and the displacements of masonry spandrels is essential for the overall results of the wall as the stiffness degradation in the spandrels is reflected on the coupling of the piers.

The typical mechanisms in spandrels observed in post-earthquake surveys are the flexural and shear failures. Shear failure shown in Figure 2 is more common in squat geometries and laterally strengthened spandrels. It is characterized with more strength that continue to build up until failure within the range of the ultimate displacement. This means that more energy dissipation is associated with the hysteretic cyclic loop representing the motion during lateral shaking. Cracks propagation has the cross x shape passing through bed and head joints at the interface between masonry units and mortar (Beyer, 2012). Flexure on the other hand shown in Figure 1 is common in slender geometries

[1] PhD Candidate, Concordia University, Montreal, Canada, hasan.ayouby@hotmail.com
[2] Professor, Chair, Concordia University, Montreal, Canada
[3] Associate Professor, Concordia University, Montreal, Canada

and spandrels with less or no lateral support. The strength endures a sudden drop at a very small displacement before it settles to the residual strength that can withstand the majority of the displacement in the spandrel until failure. Less energy dissipation is allied with this behavior due to the small hysteretic cyclic loops in the force-displacement graphs. Cracks form perpendicular to the span of the spandrel right at the corners of the opening passing through the head joints (Beyer, 2012). Hybrid cracking failure can also take place in spandrels as the formation of weak points can alter the behavior of the element.

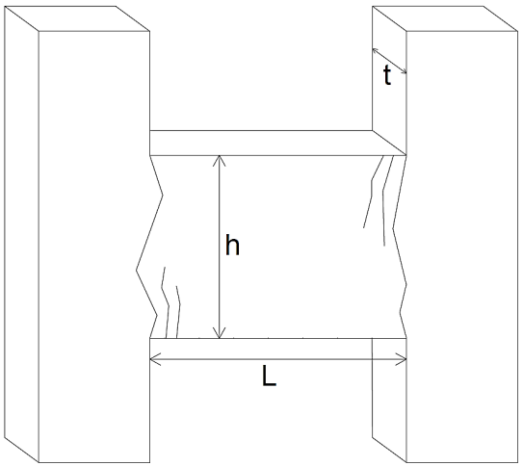

Figure 1: Flexural cracks in a spandrel

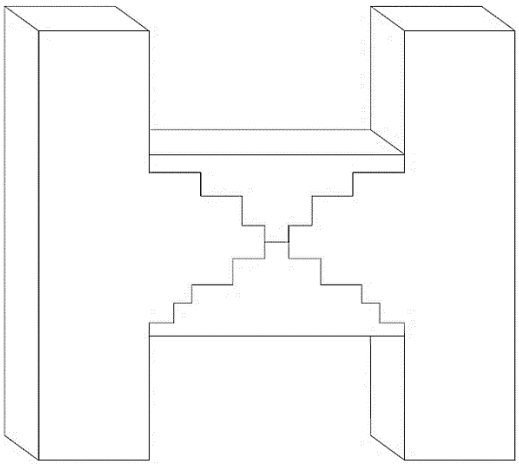

Figure 2: Shear cracks in a spandrel

Equivalent frame modeling represented in Figure 4 has proven to be a useful modeling technique that can simplify the complexity of masonry structures through reducing the number of degrees of freedom and allowing for more sophisticated analysis such as the time-history to take place (Tomazevic, 1978) & (Magenes & Della Fontana, 1998). With proper calibration of the strength formulations in the hinges sophisticated results can be delivered. Proper positioning of the flexural and shear hinges is also required as part of the model. Shear hinges are placed in the middle of the spandrel as to account for the formation of cracks at the center of element, as for the flexural hinges they are placed next to the support at the end of the rigid node following the formation of cracks at that particular zone (Pasticier, Amadio, & Fragiacomo, 2008). The moment and shear distributions along the spandrels are illustrated in Figure 3. Zero moment is assigned in the middle of the element following the assumption that the spandrel is subjected to double bending.

Parameters for masonry spandrels

The behavior of spandrels is influenced by the various parameters that characterize the spandrels. Mentioned in the previous sections are some parameters that determine the type of failure. However within each category several strength formulations are proposed throughout the literature that determine the capacity of those structural elements. The accuracy of those criterion is dependent on major parameters used in designing spandrels (Beyer & Mangalathu, 2013). The construction type of spandrels for typical practices such as using wooden lintels or masonry arches can influence the lateral behavior. Also using thick versus thin timber lintels can alter the stiffness of the element and thus the simulation results. The presence of tie rods or other lateral restricting elements can determine

the magnitude of horizontal compression forces on the spandrel. Those forces has significant implications on the type of response and developed strength within the element itself.

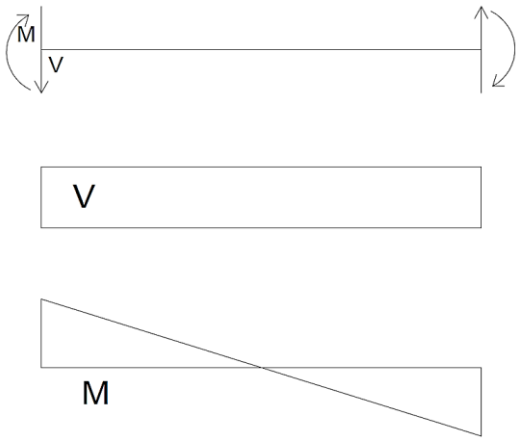

Figure 3: Shear and moment diagrams following the force distribution in spandrels

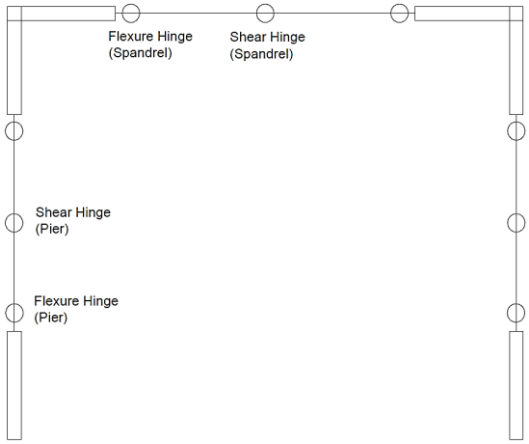

Figure 4: Distribution of plastic hinges in an equivalent frame model

We can also identify minor parameters that has indirect effect on the behavior of the spandrels. They are used to justify the variations in the results that might arise between the numerical and experimental calculations. Such parameters can include the texture of the unit masonry stones, their arrangement and material type, the thickness of the wall and the number of layers, and the type of mortar used in the construction. Also the aspect ratio of the spandrel and the scaling factors should be considered in the assessment.

An important thing to consider in the analysis is the boundary conditions that is linked to the stress distributions for shear and flexural behaviors. Since spandrels act as the connection between piers this can also affect their response as well in which reflects on the interaction between those two members and the coupling effect induced. This will be considered in the full scale model of an entire masonry wall. Instead of simplifying the model to the ones proposed by the codes mentioned earlier, it would be more satisfactory to include three cases that covers the proper connection at the peak strength of the spandrel, the weak connection at the residual strength of the spandrel and the finally the lost connection at the failure of the spandrel. Thus the piers will have fixed-fixed, intermediate and cantilever boundaries respectively.

Strength Formulations

Shear Criteria

The Italian codes (OPCM 3431, 2005) suggests the following shear criterion for the peak strength of the spandrel.

$$V_{u,1} = h.t.f_{vo} \tag{1}$$

Herein, t is the spandrel thickness, h is the height of the spandrel and f_{vo} is the shear strength of wall assemblages without considering any compression thus relying mainly on the cohesive strength of the mortar c.

Turnsek and Cacovic (Turnšek & Čačovič, 1971) suggested another formulation that accounts for the maximum tensile strength at the middle of the spandrel. The equation is borrowed from the shear strength of piers with some modifications in the parameters.

$$V_{u,2} = f_v.h.t.\beta\sqrt{1+\frac{\sigma_s}{f_v}} \quad (2)$$

Herein, f_v is the diagonal tensile strength; σ_s is the axial compressive stress; β is the aspect ratio (height/length=*h/l*) where 0.67 ≤ β ≤ 1.0.

Magenes & Della Fontana (Magenes & Della Fontana, 1998) suggested the follow criterion which influenced the one provided by the Italian codes OPCM 3431. A modification of the cohesion parameter as suggested by (Mann & Müller, 1982) is used in the calculations.

$$V_{u,3} = h.t.c_r \quad (3)$$

Where $c_r = c.\frac{1}{1+2(h_b+h_j)/(l_b+l_j)}$ is the reduced cohesion stress; h_b and h_j is are the height of the brick and the joint respectively; l_b *and* l_j are the length of the brick and the joint respectively.

Flexural Criteria

Adopted by the Italian codes OPCM 3431, the maximum shear force in a flexural governed behavior is captured by the following formulation.

$$V_{u,4} = P.\frac{h}{l}.\left[1-\frac{P}{0.85f_m ht}\right] \quad (4)$$

Where f_m is the compressive strength of the masonry; *P* is the axial force applied on the spandrel from external load. If *P* was unknown it can be replaced by the minimum of $[f_{te}\ ;\ 0.4htf_m]$; f_{te} is the tensile strength of the horizontal tension elements such as steel ties and ring beams.

The American codes FEMA 306 (FEMA 306, 1998) adopts the following equation for the flexural behavior of masonry spandrels that ignores the axial force.

$$V_{u,5} = \frac{2}{l}.\frac{2}{3}h.f_{p,tot}.\frac{h}{4(h_j+h_b)} \quad (5)$$

Where the total tensile force $f_{p,tot} = f_{t,b}.t_b.\frac{l_b}{2} + f_{t,s}.h_b.\frac{l_b}{2}.(NB-1)$; The tensile strength due to friction in the bed-joints $f_{t,b} = 0.5(0.75c + \gamma_{sp}\sigma_p)$; The tensile strength due to cohesion on the side faces of the bricks $f_{t,s} = 0.5(0.75c)$; γ_{sp} is a ratio to determine the effective vertical stress on adjacent piers suggested as 0.5; σ_p is the vertical stress on the adjacent pier; *NB* is the number of wythes; t_b is the thickness of the brick.

Cattari and Lagomarsino (Cattari & Lagomarsino, 2008) used the following equation that includes the tensile criterion at the level of the brick units.

$$V_{u,6} = \frac{2}{l}.t\left[0.85.f_m.h_c\left(\frac{h}{2}-\frac{h_c}{2}\right) + f_{tu}(h-h_c)\frac{h_c}{2}\right] \quad (6)$$

Where $f_{tu} = \min\left(\mu.\gamma_{sp}\sigma_p.\frac{l_b}{2(h_j+h_b)};\ \frac{f_{bt}}{2}\right)$ is the equivalent tensile strength in the mortar joints and the brick; f_{bt} is the limited tensile strength of the brick; γ_{sp} is suggested as 0.65; μ is the friction coefficient; $h_c = \frac{\sigma_s+f_{tu}}{0.85f_m+f_{tu}}.h$ is the depth of compressive zone.

Betti et al. (Betti, Galano, & Vignoli, 2008) also provides an equation for ultimate flexural strength in spandrels. It varies the parameters between large axial forces and small axial forces on the element shown below.

$$V_{u,7} = \frac{2}{l}.\frac{h^2 t}{6}.(kf_{tm} + \sigma_s) \quad (7)$$

Where $f_{tm} = c/2\mu$ is the tensile strength of mortar joints.

Parametric Analysis of Capacity Equations

Shear Failure Mode

In the aim of verifying the accuracy of each formulation in reference to certain parameters different experimental campaigns conducted on spandrels are selected in order to compare the numerical results to the experimental ones. A study held in Pavia, Italy focuses on two different aspects in the construction of the spandrel using full scale specimens. The samples has boundary conditions resembling the real case scenario of a spandrel in a wall built using a double-leaf Credaro stones. The preliminary characterization of the elements are represented in Table 1 (Magenes, Penna, Galasco, & Rota, 2010). Lime mortar with weak strength is used to fill the head and bed joints.

Parameters	f_m	f_v	f_t	E	G	Density
Mean Values [MPa]	3.28	0.197	0.137	2550	840	2680 kg/m^3

Table 1: Preliminary characterizations of the spandrels used in the full scale experiment

In the first experiment (F Graziotti, Magenes, & Penna, 2012) the parameter tested is the presence and absence of lateral support. Two samples are built with dimensions l x h x t (length; height; thickness) = 1200x1080x320mm with a thick lintel with height of 120mm using two wythes. The first sample named W1 has no lateral support while the other sample W2 has a lateral support exerting an axial force F=38KN. The second experiment (Francesco Graziotti, Penna, & Magenes, 2014) tests the variation in the size of the lintels used to support the masonry units at the bottom of the structural element while utilizing and initial axial force of 28KN. The spandrels have dimensions l x h x t = 1200x780x320mm. The first sample W3 has a thick wooden lintel with 120mm depth while the second sample W4 has a thin wooden lintel with depth of 25mm. The type of failure associated with each parameter the maximum and residual strength obtained are summarized in Table 2. It has to be noted that there was a problem with the actuator while testing W4 that might alter the results. V_u represent the maximum shear force reached by the spandrel. Specimen W1 exhibit a flexural failure mode and thus would be excluded from this analysis.

Specimen	V_u [KN]	Failure Mode
W2	60	Diagonal Shear
W3	38	Diagonal Shear
W4	23	Hybrid

Table 2: Experimental results from the in-plane cyclic tests on the piers

The values of the cohesion strength *c* and the friction coefficient μ_s are chosen to be 0.35 MPa and 0.65 respectively, based on Elmenshawi literature (Elmenshawi & Shrive, 2015). The irregular stones have a length of 200-350mm and height of 100-150mm with mortar joints thickness ranging between 20-30mm. Average values are used. The height of the wooden lintel isn't considered in the calculation of the spandrel's height. The results of maximum shear forces estimated by the simplified equations are mentioned in Table 3.

	Equation 1	Equation 2	Equation 3
Parameters	**$V_{u,1}$ [KN]**	**$V_{u,2}$ [KN]**	**$V_{u,3}$ [KN]**
W2	120.9	61.3	60.5
W3	87.4	32.0	43.7
W4	87.4	32.0	43.7

Table 3: Results of maximum shear from the simplified formulations

In another study (Knox, Dizhur, & Ingham, 2017) six URM brick masonry frames are tested for in-plane cyclic behavior. Full scale specimens are constructed using 80 years old bricks with typical dimensions of 225x108x75mm for length, width and height respectively and weak lime mortar of 2.9MPa compressive strength and 10mm thickness of mortar joints.

Parameters	**f_v**	**f_t**	**μ**	**c**
Mean Values [MPa]	0.262	0.185	0.7	0.3

Table 4: Mechanical properties of the masonry panels

Different dimensions l x h x t of the spandrels summarized in Table 5 are varied between the samples with some variations in the axial stresses on the piers holding the spandrels along with the experimental shear forces and the failure modes. Sample S3 and S5 has same dimensions but the axial stresses on the adjacent piers are higher in S3. The mechanical properties of the materials are listed in Table 4. Zero axial forces are applied on the spandrels. It should be noted that the height of the piers in specimen S6 is less than the rest of the samples.

Specimen	**Dimensions [mm]**	**V_u [KN]**	**Failure Mode**
S1	1240x590x230	83.6	Diagonal Shear
S2	1740x590x230	49.3	Diagonal Shear
S3	1240x940x230	83.2	Diagonal Shear
S4	1240x1260x230	89.7	Diagonal Shear
S5	1240x940x230	48.6	Diagonal Shear
S6	1240x1450x230	24.9	Diagonal Shear

Table 5: Experimental results from the in-plane cyclic tests on the piers

Applying the parameters to the simplified equations, different estimations of the maximum shear forces are extracted and summarized in Table 6.

	Equation 1	Equation 2	Equation 3
Parameters	**$V_{u,1}$ [KN]**	**$V_{u,2}$ [KN]**	**$V_{u,3}$ [KN]**
S1	40.7	16.8	23.6
S2	40.7	12.0	23.6
S3	64.9	42.6	37.6
S4	86.9	76.6	50.4
S5	64.9	42.6	37.6
S6	100.1	101.4	58.1

Table 6: Results of maximum shear from the simplified formulations

To compare the experimental and numerical results of maximum shear forces attained by the spandrels, the ratios of experimental to numerical forces are displayed in Table 7 for all the previous samples considered in this study. The values closer to 1 shows good correlations.

Ratio	$V_u/V_{u,1}$	$V_u/V_{u,2}$	$V_u/V_{u,3}$
W2	0.50	0.98	0.99
W3	0.43	1.19	0.87
W4	0.26	0.72	0.53
S1	2.05	4.98	3.54
S2	1.21	4.11	2.09
S3	1.28	1.95	2.21
S4	1.03	1.17	1.78
S5	0.75	1.14	1.29
S6	0.25	0.25	0.43

Table 7: Ratio of experimental to the numerical shear capacity values

It is evident from the shear ratios that Equations 2 & 3 can simulate the experimental results to a very good extent while Equation 1 over estimates the forces by almost double the values. Figure 5 shows that the equations better represent the values at lower axial forces. The shear forces in Figure 6 are similar in both thick and thin lintels which indicates the deficiency of the formulations in considering such a variable in the calculations.

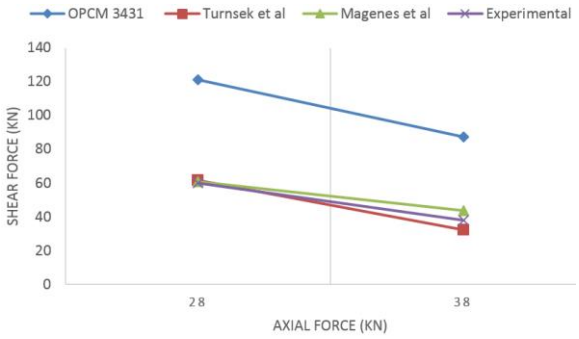

Figure 5: Variation of shear force with respect to the axial force in spandrels W2 & W3

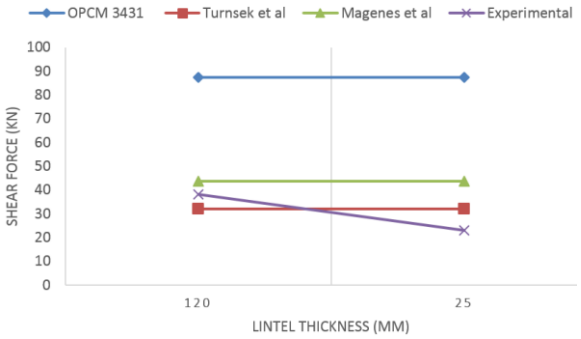

Figure 6: Variation of shear force with respect to the thickness of lintels in spandrels W3 & W4

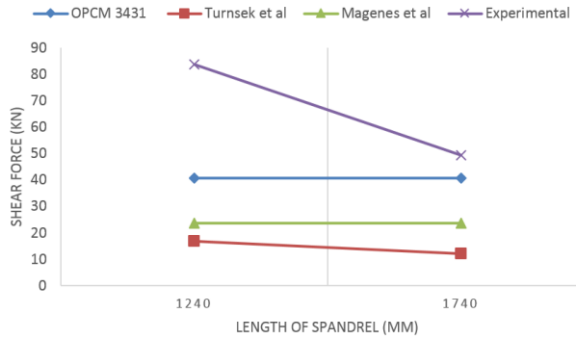

Figure 7: Variation of shear force with respect to the length of spandrels S1 & S2

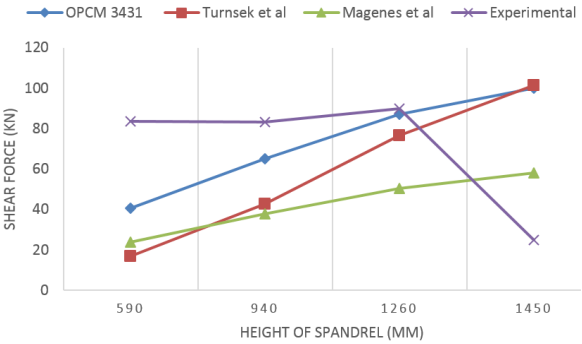

Figure 8: Variation of shear force with respect to the height of spandrels S1, S3, S4 & S6

Observing the shear ratios for the second campaign, a huge divergence in the results is recognized for most of the samples. Equation 1 gives good correlation for specimen S4 while Equation 2 gives fair correlation to specimen S5 with 14% divergence. In Figure 7 it can be seen that Equation 1 and

3 have same shear force values at both lengths of the spandrels indicating a deficiency in including this variable. In general the results are better simulated for higher length of the spandrels. Observing Figure 8, the equations are yielding better results with the increase in the height of the spandrels apart from the last value at 1450mm which experiences a sudden drop in the experimental shear forces that can be justified by the variations in the pier length used in that sample. In general Equation 1 had better results than the other equations. It should be noted that the variation in the vertical stresses on the adjacent piers represented in samples S3 and S5 cannot be captured by the suggested equations in the literature.

Flexural Failure Mode

Three specimens from three different experimental campaigns with flexural failure are selected to conduct the comparisons. Due to the scarcity of data related to flexural behavior in spandrels the parameters are chosen roughly for the most convenient representation. Sample W1 from the previous section will be used (F Graziotti et al., 2012). Another sample M1 is utilized constructed using a thick lintel of 120mm height and no axial forces. It is constructed using brick masonry with dimensions 250x120x55mm. Finally a third sample T1 is selected (Beyer & Dazio, 2012) constructed using a thick lintel of 140mm height and brick masonry with typical dimensions of 250x120x60mm. A variable axial force is applied on the spandrel depending on the horizontal elongation starting with 5KN as initial force and reaching 67KN at the final failure with maximum crack. All the dimensions of the specimens and the experimental shear capacities are listed in Table 8.

Specimen	Dimensions [mm]	V_u [KN]	Failure Mode
W1	1200x1080x320	32	Flexural Failure
M1	1000x1080x380	70	Flexural Failure
T1	1180x1120x380	82	Flexural Failure

Table 8: Experimental data from the in-plane cyclic tests on the piers

The mechanical properties of all three samples are summarized in Table 9. The data needed to apply the formulations are inferred from the same experimental campaigns where the specimens are tested or from similar samples from other sources when the data is missing (Brignola, Frumento, Lagomarsino, & Podestà, 2008).

Parameters	f_m [MPa]	μ	c [MPa]	NB	f_{bt} [MPa]	h_j [mm]	σ_p [MPa]	σ_s [MPa]
W1	3.28	0.65	0.35	2	19	25	0.17	0
M1	4	0.85	0.35	3	7	10	0.5	0
T1	4	0.85	0.35	2	7	10	0.33	0.16

Table 9: Mechanical parameters for the selected samples

The parameters are defined previously along with the formulations. In the same manner for shear analysis, the numerical capacity values associated with flexural failure are viewed in Table 10.

	Equation 4	Equation 5	Equation 6	Equation 7
Parameters	$V_{u,4}$ [KN]	$V_{u,5}$ [KN]	$V_{u,6}$ [KN]	$V_{u,7}$ [KN]
W1	-	12.6	20.0	27.9
M1	-	30.6	203.7	30.4
T1	63.6	21.2	170.6	49.3

Table 10: Numerical capacity values for spandrels associated with flexural failure

In order to compare the numerical to the experimental values the ratios shown in Table 11 are derived.

Ratio	$V_u/V_{u,4}$	$V_u/V_{u,5}$	$V_u/V_{u,6}$	$V_u/V_{u,7}$
W1	-	2.54	1.6	1.15
M1	-	2.29	0.34	2.30
T1	1.29	4.01	0.48	1.66

Table 11: Ratio of experimental to the numerical shear capacity values

Analyzing the results it is clear that the formulations can hardly represent the experimental tests. Equation 8 is able to give fair simulation for sample W1 with 15% divergence. In all other cases there is a huge divergence in the capacity results from the equations. The parameters involved in this study are the variations in the height of the spandrel between W1 and M1, the variation in the material type of the stone units between W1 and T1, and the application if axial force in case if T1. Given the limitations in the information due to the small number of samples it can be derived that the performance of the equations has to be revised. The divergence reaching more than 100% in certain cases raises red flags on the competency of those formulation and their ability to compute the capacity of spandrels.

Conclusion

The variation in the parameters between unreinforced masonry constructions indicates the necessity to verify their influence on the behavior of the elements in seismic action. It is realized from the literature of performed experimental campaigns that the failures in spandrels associated with shear cracks are more common than those associated with flexural cracks. This explains the fact that the parametric study in this work has more data to evaluate the shear formulations. Each equation from different codes or suggested by researchers is yielding different results showing that the calibration process to which the equations are proposed has a massive impact on its performance. In the first part of the study regarding shear failure mode the effect of the axial force, lintel thickness, length of the spandrel and height of the spandrel is considered. It is shown that the simulations are better at lower axial forces, lower lintel thicknesses and higher heights of spandrels while it remains indifferent for the length of the spandrels. It is also derived that Equations 2 & 3 perform better for stone unit samples in comparison to the brick unit samples, while the relations swaps for Equation 1. In the second part of the study related to the flexural failure mode, the amount of samples found in the literature wasn't enough to yield any deduction which shows the need for more experimental tests on spandrels. In general there is a lot of divergence in the results for all the parameters involved. Also Equation 4 is not reliable for samples without axial forces. As more data are acquired it would reveal a better connection between the different parameters of spandrels and the suggested equations which will help in refining the modeling approach utilized by decreasing the size of the error generated and encompassing a bigger number of parameters.

Acknowledgments

The financial support provided by Concordia University and IC-Impacts Research Centre of Excellence Network Canada is gratefully acknowledged.

References

Betti, M., Galano, L., & Vignoli, A. (2008). Seismic Response Of Masonry Plane Walls: A Numerical Study On Spandrel Strength. *AIP*. Presented at the 2008 seismic engineering conference commemorating the 1908 Messina and Reggio Calabria earthquake, Reggio Calabria, Italy.

Beyer, K. (2012). Peak and residual strengths of brick masonry spandrels. *Engineering Structures*, *41*, 533–547. https://doi.org/10.1016/j.engstruct.2012.03.015

Beyer, K., & Dazio, A. (2012). Quasi-Static Cyclic Tests on Masonry Spandrels. *Earthquake Spectra*, *28*(3), 907–929. https://doi.org/10.1193/1.4000063

Beyer, K., & Mangalathu, S. (2013). Review of strength models for masonry spandrels. *Bulletin of Earthquake Engineering*, *11*(2), 521–542. https://doi.org/10.1007/s10518-012-9394-3

Brignola, A., Frumento, S., Lagomarsino, S., & Podestà, S. (2008). Identification of Shear Parameters of Masonry Panels Through the In-Situ Diagonal Compression Test. *International Journal of Architectural Heritage*, *3*(1), 52–73. https://doi.org/10.1080/15583050802138634

Cattari, S., & Lagomarsino, S. (2008). A strength criterion for the flexural behaviour of spandrels in un-reinforced masonry walls. *14th World Conference on Earthquake Engineering*. Presented at the Beijing, China. Beijing, China.

Elmenshawi, A., & Shrive, N. (2015). Assessment of Multi-Wythe Stone Masonry Subjected to Seismic Hazards. *Journal of Earthquake Engineering*, *19*(1), 85–106.

FEMA 306. (1998). *Evaluation of Earthquake-Damaged Concrete and Masonry Wall Buildings*. Washington DC: ATC.

Foraboschi, P. (2009). Coupling effect between masonry spandrels and piers. *Materials and Structures*, *42*(3), 279–300. https://doi.org/10.1617/s11527-008-9405-7

Graziotti, F, Magenes, G., & Penna, A. (2012). *Experimental cyclic behaviour of stone masonry spandrels*. 10. Lisboa.

Graziotti, Francesco, Penna, A., & Magenes, G. (2014). *Influence of timber lintels on the cyclic behaviour of stone masonry spandrels*. Presented at the 9th International Masonry Conference, Guimaraes.

Knox, C. L., Dizhur, D., & Ingham, J. M. (2017). Experimental Cyclic Testing of URM Pier-Spandrel Substructures. *Journal of Structural Engineering*, *143*(2), 04016177. https://doi.org/10.1061/(ASCE)ST.1943-541X.0001650

Magenes, G., & Della Fontana, A. (1998). *Simplified non-linear seismic analysis of masonry buildings*. *8*. London, UK.

Magenes, G., Penna, A., Galasco, A., & Rota, M. (2010, January 1). *Experimental Characterisation of Stone Masonry Mechanical Properties*. Presented at the 8th International Masonry Conference, Dresden.

Mann, W., & Müller, H. (1982). Failure of Shear-Stressed Masonry- an Enlarged Theory, Tests and Application to Shear Walls. *British Ceramic Society*, *30*, 223–235.

OPCM 3431. (2005). *Ulteriori modifiche ed integrazioni all OPCM 3274/03 (in Italian)*.

Pasticier, L., Amadio, C., & Fragiacomo, M. (2008). Non-linear seismic analysis and vulnerability evaluation of a masonry building by means of the SAP2000 V.10 code. *Earthquake Engineering & Structural Dynamics*, *37*(3), 467–485.

Tomazevic, M. (1978). *The Computer Program POR* [Report ZRMK]. Ljubljana, Slovenian.

Turnšek, V., & Čačovič, F. (1971). *Some experimental results on the strength of brick masonry walls*. Presented at the 2nd International Brick-Masonry Conference, British Ceramic Society, Stoke-on-Trent.